Phasor Analytical Model of Non-isolated DC/DC Converter Based on Modular Multilevel Converter for DC Transmission Grids

A. Jamshidi Far, *Member, IEEE*, and D. Jovcic, *Fellow, IEEE*

Abstract—Non-isolated DC/DC converter based on modular multilevel converter（MMC）technology is expected to play an important role in future DC transmission grids. This paper presents a phasor analytical model for this new family of converters which is suitable for a range of studies like DC grid power flow or DC/DC parametric design. The 30th-order phasor model is derived in 3 coordinate frames: zero sequence (DC), fundamental frequency (*dq*), and double frequency (*d2q2*). The second-harmonic current suppression control is included as an option. Additionally, an estimation of the required control signals is presented, and a closed-loop model is developed which facilitates direct calculation of all variables and fast parametric studies. The accuracy of the proposed models is verified against a detailed PSCAD model for a wide range of parameters. The studies illustrate the importance of the second-harmonic components on the model accuracy. Finally, the impact of the converter parameters on the performance is studied, and a basic eigenvalue stability analysis is given.

Index Terms—High-voltage direct current (HVDC) transmission, modular multilevel converter (MMC), non-isolated DC/DC converter, phasor modelling.

I. INTRODUCTION

THE first high-voltage direct current (HVDC) transmission grid has been implemented in China recently, as a significant advance of point-to-point HVDC transmission [1]. DC transmission grids enable reliable, flexible, and secure integration of multiple large renewable energy sources with national transmission systems [1], [2].

DC/DC converters are expected to play a significant role in future DC transmission grids [3]. CIGRE has studied DC/DC converters in the first working group on the feasibility of DC grids [4], and then on power flow controllers in the analysis of DC grid control [5]. Recently, CIGRE WG B4.76 has published its report on DC/DC converters [6]. In general, these converters enable power trading between two DC systems with different (or equal) voltage levels with addition-al attractive features like bidirectional power flow control, DC fault isolation, and stabilization and elimination of interoperability issues [2]. There are two main families of DC/DC converters: ① isolated converter based on two-stage DC/AC/DC conversion which is known from low-power applications; and ② the new non-isolated converter which uses single-stage conversion with less semiconductors and lower costs [7].

The operating principle of non-isolated MMC DC/DC converter (NIMDC) has been presented in [8], and a comprehensive overview of it for medium-voltage DC (MVDC) and HVDC applications is given in [9]. CIGRE WG B4.76 proposes a 600 MW 320 kV/250 kV NIMDC test case [6], [10] and the studies conclude that the components and ratings will be comparable to a similar MMC AC/DC converter. These results raise expectations that the NIMDC potentially offers a very cost-effective method of interchanging the power between two HVDC systems and is more attractive than using the isolated DC/DC converter in many applications.

Phasor converter models belong to the family of average models and have been applied to a range of converter topologies such as MMC AC/DC converters [11]. Phasor-domain converter models use *dq* components of all variables assuming that the frequency is constant. If the system dynamics are considered, dynamic phasor models are obtained, while neglecting the dynamics will lead to steady-state phasor models [12]. The focus of this paper is on the steady-state phasor models which are suitable for a wide range of power system studies in steady state as well as converter parametric studies related to design and control.

A steady-state phasor-domain NIMDC model is developed in [13] and used for converter design as well as developing control methods in [14]. However, the model in [13] is overly simplified, and its accuracy has not been evaluated. It is only based on DC and fundamental-frequency components without considering the second harmonic or the interactions between coordinate frames. And it assumes identical parameters for upper and lower arms. The application area of this model is very limited. Reference [15] presents a linearized small-signal state-space model which is similarly oversimplified and has not been tested for accuracy. The shortcomings of these models will be demonstrated, and a systematic accurate modelling approach will be presented and verified in this paper.

Based on literature review, there is a need for an accurate analytical model for NIMDC, which would facilitate fast de-

sign and parametric studies of component stress/selection and performance. The optimal design of NIMDC is challenging because of numerous internal parameters such as operating frequency, arm inductances, and cell capacitances, which is unlike that of common MMC AC/DC converter and differs between upper and lower arms.

It is known that electromagnetic topology (EMT) time-domain simulation of DC/DC converters is difficult since higher operating frequency implies very small simulation steps, and may cause simulation accuracy or instability issues [16]. An analytical model facilitates faster parametric studies and provides better insight into design principles. Additionally, phasor model can be used for fast power flow studies, which may involve numerous converters in future large DC grids.

This paper contributes with an accurate phasor model for NIMDC by considering the DC, fundamental-frequency, and second-harmonic components of the key variables of the converter (arm sum voltage, arm voltage, and arm current) for upper and lower arms. The model is developed in 3 coordinate frames and the interactions among them are considered. The analytical model is validated against detailed PSCAD model using several realistic GW-size test systems. The importance of key modelling principles to the model accuracy is highlighted. The use of this model will finally be illustrated on a study of parametric design.

II. NIMDC

A. Converter Structure

Figure 1 shows the structure of a unipolar three-phase NIMDC [2], and another symmetrical converter would be needed for bipolar topology, where V_1 and V_2 are the DC voltages at high voltage (HV) and low voltage (LV) sides, respectively.
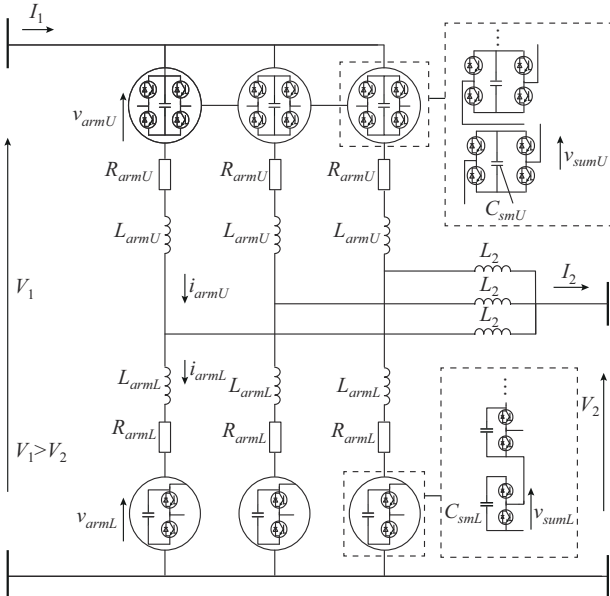

Fig. 1. Structure of a unipolar three-phase NIMDC.

This topology has substantially different upper (denoted by subscript U) and lower (denoted by subscript L) arms (in terms of cell topology, parameters, and control), because the

contribution of upper and lower arms in the amount of power transfer is different and depends on the voltage step ratio [10]. This implies that different values for the cell capacitors and arm inductors should be selected to keep the arm voltage ripple almost the same, and to have almost the same limit for the AC currents of the arms under normal operating conditions and the currents rise in case of DC fault. Each lower arm includes N half-bridge cells. Upper arms also have N half-bridge cells, and a number of half-bridge cells should be of full-bridge type to provide fault blocking capability [10].

B. Operating Principle

The operating principles are described in [8], and only a brief summary is provided here. The number of phase-legs can be $p \geq 2$ for HVDC applications, which depends on the required rating of NIMDC power or current.

The voltage and current of each arm are composed of a DC component and an AC component. Upper arms have DC components of voltage and current approximately equal to $V_1 - V_2$ and lower-arm DC current I_1/p, respectively, while the lower-arm DC voltage is V_2 and the lower-arm DC current is $(I_1 - I_2)/p$, where I_1 and I_2 are the DC currents at HV and LV sides, respectively. Because of different DC power on upper and lower arms, it is necessary to introduce power balancing using AC power at fundamental frequency ω. Under a balanced operating condition, the AC component of the voltage or current among the p phase-legs has identical amplitude with the phase angles displaced by $2\pi/p$. As a consequence of non-linear nature of MMC-arm voltage control, a second harmonic will appear on the arm voltages and currents.

C. Time-domain Dynamic Equations

The dynamic equations of the NIMDC are studied in [8] and only a summary is given here. The basic dynamic equations for arm currents i_{armU} and i_{armL}, arm sum voltages v_{armU}^{Σ} and v_{armL}^{Σ}, and arm voltages v_{armU} and v_{armL} are:

$$\begin{cases} \dfrac{\mathrm{d}i_{armU}(t)}{\mathrm{d}t} = \dfrac{-L_{yL}}{L_Z} v_{armU}(t) - \dfrac{L_2}{L_Z} v_{armL}(t) - \dfrac{L_{yL}R_{armU}}{L_Z} i_{armU}(t) - \\ \qquad \dfrac{L_2 R_{armL}}{L_Z} i_{armL}(t) + \dfrac{1}{L_Z}\left(L_{yL}V_1 - L_{armL}V_2\right) \\ \dfrac{\mathrm{d}i_{armL}(t)}{\mathrm{d}t} = -\dfrac{L_2}{L_Z} v_{armU}(t) - \dfrac{L_{yU}}{L_Z} v_{armL}(t) - \dfrac{L_2 R_{armU}}{L_Z} i_{armU}(t) - \\ \qquad \dfrac{L_{yU}R_{armL}}{L_Z} i_{armL}(t) + \dfrac{1}{L_Z}\left(L_2 V_1 + L_{armU}V_2\right) \end{cases}$$
(1)

$$\begin{cases} \dfrac{\mathrm{d}v_{armU}^{\Sigma}(t)}{\mathrm{d}t} = \dfrac{1}{C_{armU}} m_U(t) i_{armU}(t) \\ \dfrac{\mathrm{d}v_{armL}^{\Sigma}(t)}{\mathrm{d}t} = \dfrac{1}{C_{armL}} m_L(t) i_{armL}(t) \end{cases}$$
(2)

$$\begin{cases} v_{armU}(t) = m_U(t) v_{armU}^{\Sigma}(t) \\ v_{armL}(t) = m_L(t) v_{armL}^{\Sigma}(t) \end{cases}$$
(3)

where L_{armU} and L_{armL} are the upper- and lower-arm induc-

tances, respectively; L_2 is the output filter; C_{armU} and C_{armL} are the upper- and lower-arm equivalent capacitances, respectively; R_{armU} and R_{armL} are the upper- and lower-arm equivalent resistances, respectively; and m_U and m_L are the upper- and lower-arm control signals, respectively. And some new parameters are introduced as:

$$\begin{cases} L_z = L_2\left(L_{armU} + L_{armL}\right) + L_{armU}L_{armL} \\ L_{yU} = L_2 + L_{armU} \\ L_{yL} = L_2 + L_{armL} \\ C_{armU} = \dfrac{C_{smU}}{N} \\ C_{armL} = \dfrac{C_{smL}}{N} \end{cases} \quad (4)$$

where C_{smU} and C_{smL} are the upper- and lower-arm cell capacitances, respectively; and N is the number of submodules (SM) in arm.

III. NIMDC PHASOR EQUATIONS IN *DQ* FRAME

The aim of this parametric analytical model is to obtain all the NIMDC steady-state variables (voltages and currents), which are dependent on converter parameters, operating conditions, and control signals. The time-domain equations (1)-(3) are converted to phasor domain, which is contrary to conventional phasor modelling where only fundamental frequency (50 Hz) terms are considered. Modelling this converter requires 3 coordinate frames: zero-sequence (DC), fundamental frequency (*dq*), and second harmonic (*d2q2*). It is worth noting that the fundamental frequency here is a design parameter and is usually in the range of several hundred hertz [10]. A challenge is to represent non-linear terms in (2) and (3) since each variable contains multiple components from different coordinate frames. Phasor modelling of NIMDC includes the following steps.

Step 1: express each of the variables from (1)-(3) in the 3 coordinate frames which will have 5 (1 in DC, 2 in *dq*, and 2 in *d2q2*) components in general case.

Step 2: replace each of the variables (considering all components) in (1)-(3) and perform multiplications. When variables from different coordinate frames are multiplied, it is necessary to consider rules for *dq* frame modelling [2], [11].

Step 3: separate each of the variables in (1)-(3) in zero-sequence, fundamental-frequency, and second-harmonic frames.

Although the converter shown in Fig. 1 is a three-phase NIMDC, the proposed modelling method can be applied to a *p*-phase NIMDC as long as the *p*-phase system is symmetrical and balanced to enable the transformation to an orthogonal coordinate system [17], [18].

A. Assumptions for Variables

It is assumed that all NIMDC parameters and variables are symmetrical and balanced. The control signals are assumed to have zero-sequence and fundamental frequency components only:

$$\begin{cases} m_U(t) = M_{U0} + M_U \cos(\omega t) = \left(M_{U0}\right)_0 + \left(M_U\right)_d \\ m_L(t) = M_{L0} + M_L \cos\left(\omega t + \phi_{m_L}\right) = \left(M_{L0}\right)_0 + \left(M_{Ld}\right)_d + \left(M_{Lq}\right)_q \end{cases} \quad (5)$$

where M_U and M_L are the control signals for the NIMDC without second-harmonic current suppression control (SHC-SC); ϕ_{m_L} is the phase shift; the subscript 0 denotes the zero-sequence component; and the subscripts d and q denote the two components in the coordinate frame rotating at the fundamental frequency $\omega = 2\pi f$ (determined by the converter operating frequency f). The fundamental-frequency component of the upper-arm control signal is aligned with the d-axis of dq coordinate frame, i.e., $\phi_{m_U} = 0$, and therefore, $\left(M_U\right)_q = 0$ and $\left(M_{Ud}\right)_d = \left(M_U\right)_d$.

The upper- and lower-arm currents are assumed to have the components in 3 frames as zero sequence, fundamental frequency, and second harmonic:

$$\begin{cases} i_{armU}(t) = \left(I_{U0}\right)_0 + \left(I_{Ud}\right)_d + \left(I_{Uq}\right)_q + \left(I_{Ud2}\right)_{d2} + \left(I_{Uq2}\right)_{q2} \\ i_{armL}(t) = \left(I_{L0}\right)_0 + \left(I_{Ld}\right)_d + \left(I_{Lq}\right)_q + \left(I_{Ld2}\right)_{d2} + \left(I_{Lq2}\right)_{q2} \end{cases} \quad (6)$$

where I_U and I_L are the upper- and lower-arm currents, respectively. The subscripts $d2$ and $q2$ denote the two components in the coordinate frame rotating at the second-harmonic 2ω. The multiplication terms in (2) and (3) generate higher harmonics. However, only second-harmonic terms are considered in this paper because of their significant importance on the model accuracy as verified in Section V, and the higher harmonics are neglected.

The time-domain expression will be omitted for brevity, but it can be derived for each variable as in (5).

The upper- and lower-arm sum voltages are also assumed to have zero-sequence, fundamental-frequency, and second-harmonic components, and presented as below:

$$\begin{cases} v_{armU}^{\Sigma}(t) = \left(V_{U0}^{\Sigma}\right)_0 + \left(V_{Ud}^{\Sigma}\right)_d + \left(V_{Uq}^{\Sigma}\right)_q + \left(V_{Ud2}^{\Sigma}\right)_{d2} + \left(V_{Uq2}^{\Sigma}\right)_{q2} \\ v_{armL}^{\Sigma}(t) = \left(V_{L0}^{\Sigma}\right)_0 + \left(V_{Ld}^{\Sigma}\right)_d + \left(V_{Lq}^{\Sigma}\right)_q + \left(V_{Ld2}^{\Sigma}\right)_{d2} + \left(V_{Lq2}^{\Sigma}\right)_{q2} \end{cases} \quad (7)$$

Similarly, the upper- and lower-arm voltages are:

$$\begin{cases} v_{armU}(t) = \left(V_{U0}\right)_0 + \left(V_{Ud}\right)_d + \left(V_{Uq}\right)_q + \left(V_{Ud2}\right)_{d2} + \left(V_{Uq2}\right)_{q2} \\ v_{armL}(t) = \left(V_{L0}\right)_0 + \left(V_{Ld}\right)_d + \left(V_{Lq}\right)_q + \left(V_{Ld2}\right)_{d2} + \left(V_{Lq2}\right)_{q2} \end{cases} \quad (8)$$

B. Zero-sequence Model

Considering only zero-sequence terms for all arm voltages and currents (the first component of (6) and (8)), equating the differential terms to zero and using the second sub-equation of (4), the zero-sequence expression of (1) is:

$$\begin{cases} V_{U0} = V_1 - V_2 - R_{armU}I_{U0} \\ V_{L0} = V_2 - R_{armL}I_{L0} \end{cases} \quad (9)$$

Using the *dq* modelling algebra ((43) in [11]), the zero-sequence expression of (2) can be obtained in a similar manner as:

$$\begin{cases} \left(\dfrac{dv_{armU}^{\Sigma}(t)}{dt}\right)_0 = \left(m_U(t)i_{armU}(t)\right)_0 \Rightarrow 0 = M_{U0}I_{U0} + \dfrac{M_U I_{Ud}}{2} \\ \left(\dfrac{dv_{armL}^{\Sigma}(t)}{dt}\right)_0 = \left(m_L(t)i_{armL}(t)\right)_0 \Rightarrow \\ \qquad\qquad 0 = M_{L0}I_{L0} + \dfrac{M_{Ld}I_{Ld}}{2} + \dfrac{M_{Lq}I_{Lq}}{2} \end{cases} \tag{10}$$

It is observed that the upper-arm equation can be derived from the lower-arm one by replacing the subscript U with L and considering $M_{Uq}=0$ and $M_{Ud}=M_U$. From now on, only lower-arm equations are derived for brevity.

It is also observed that the variables from two coordinate frames are presented in the above equation, due to the interaction between the zero-sequence and fundamental-frequency coordinate frames. If a simple modelling is adopted as in [13], only the first term is considered and the accuracy is reduced.

The zero-sequence expression of the lower-arm equation of (3) is obtained similarly as:

$$\left(v_{armL}(t)\right)_0 = \left(m_L(t)v_{armL}^{\Sigma}(t)\right)_0 \Rightarrow V_{L0} = M_{L0}V_{L0}^{\Sigma} + \dfrac{M_{Ld}V_{Ld}^{\Sigma}}{2} + \dfrac{M_{Lq}V_{Lq}^{\Sigma}}{2} \tag{11}$$

C. Fundamental-frequency Model

Using the *dq* algebra for differential equation ((45) in [11]), the differential terms of the lower arm of (1) can be expressed in *dq* frame as:

$$\left(\dfrac{di_{armL}(t)}{dt}\right)_{dq} = \left(-k\omega I_{Lq}\right)_d + \left(k\omega I_{Ld}\right)_q \tag{12}$$

where $k=1$ for the fundamental frequency, and $k=2$ for the second harmonic.

The fundamental frequency expression of (1) is then obtained by replacing (12) in the left side of (1), and by considering only the fundamental-frequency components of the arm voltages and currents as:

$$\begin{cases} \left(-\omega I_{Uq}\right)_d + \left(\omega I_{Ud}\right)_q = \\ \qquad \left(\dfrac{-L_{yL}}{L_Z}V_{Ud} + \dfrac{-L_2}{L_Z}V_{Ld} + \dfrac{-L_{yL}R_{armU}}{L_Z}I_{Ud} + \dfrac{-L_2 R_{armL}}{L_Z}I_{Ld}\right)_d + \\ \qquad \left(\dfrac{-L_{yL}}{L_Z}V_{Uq} + \dfrac{-L_2}{L_Z}V_{Lq} + \dfrac{-L_{yL}R_{armU}}{L_Z}I_{Uq} + \dfrac{-L_2 R_{armL}}{L_Z}I_{Lq}\right)_q \\ \left(-\omega I_{Lq}\right)_d + \left(\omega I_{Ld}\right)_q = \\ \qquad \left(\dfrac{-L_2}{L_Z}V_{Ud} + \dfrac{-L_{yU}}{L_Z}V_{Ld} + \dfrac{-L_2 R_{armU}}{L_Z}I_{Ud} + \dfrac{-L_{yU}R_{armL}}{L_Z}I_{Ld}\right)_d + \\ \qquad \left(\dfrac{-L_2}{L_Z}V_{Uq} + \dfrac{-L_{yU}}{L_Z}V_{Lq} + \dfrac{-L_2 R_{armU}}{L_Z}I_{Uq} + \dfrac{-L_{yU}R_{armL}}{L_Z}I_{Lq}\right)_q \end{cases} \tag{13}$$

The fundamental frequency expression of (2) and (3) can be expressed similarly as:

$$\begin{aligned} \left(-\omega C_{armL}V_{Lq}^{\Sigma}\right)_d + &\left(\omega C_{armL}V_{Ld}^{\Sigma}\right)_q = \\ &\left(M_{L0}I_{Ld} + M_{Ld}I_{L0} + \dfrac{M_{Ld}I_{Ld2}}{2} + \dfrac{M_{Lq}I_{Lq2}}{2}\right)_d + \\ &\left(M_{L0}I_{Lq} + M_{Lq}I_{L0} - \dfrac{M_{Lq}I_{Ld2}}{2} + \dfrac{M_{Ld}I_{Lq2}}{2}\right)_q \end{aligned} \tag{14}$$

$$\begin{aligned} \left(V_{Ld}\right)_d + &\left(V_{Lq}\right)_q = \\ &\left(M_{Ld}V_{L0}^{\Sigma} + M_{L0}V_{Ld}^{\Sigma} + \dfrac{M_{Ld}V_{Ld2}^{\Sigma}}{2} + \dfrac{M_{Lq}V_{Lq2}^{\Sigma}}{2}\right)_d + \\ &\left(M_{Lq}V_{L0}^{\Sigma} + M_{L0}V_{Lq}^{\Sigma} - \dfrac{M_{Lq}V_{Ld2}^{\Sigma}}{2} + \dfrac{M_{Ld}V_{Lq2}^{\Sigma}}{2}\right)_q \end{aligned} \tag{15}$$

Each of the above equations will lead to two equations (one along each of the *dq* axes).

D. Second-harmonic Model

The two equations in (1) are expressed in the second-harmonic frame using (12) with $k=2$ for the left side and by considering only the second harmonic of the arm voltages and currents at the right side as:

$$\begin{cases} \left(-2\omega I_{Uq2}\right)_{d2} + \left(2\omega I_{Ud2}\right)_{q2} = \\ \quad \left(\dfrac{-L_{yL}}{L_Z}V_{Ud2} + \dfrac{-L_2}{L_Z}V_{Ld2} + \dfrac{-L_{yL}R_{armU}}{L_Z}I_{Ud2} + \dfrac{-L_2 R_{armL}}{L_Z}I_{Ld2}\right)_{d2} + \\ \quad \left(\dfrac{-L_{yL}}{L_Z}V_{Uq2} + \dfrac{-L_2}{L_Z}V_{Lq2} + \dfrac{-L_{yL}R_{armU}}{L_Z}I_{Uq2} + \dfrac{-L_2 R_{armL}}{L_Z}I_{Lq2}\right)_{q2} \\ \left(-2\omega I_{Lq2}\right)_{d2} + \left(2\omega I_{Ld2}\right)_{q2} = \\ \quad \left(\dfrac{-L_2}{L_Z}V_{Ud2} + \dfrac{-L_{yU}}{L_Z}V_{Ld2} + \dfrac{-L_2 R_{armU}}{L_Z}I_{Ud2} + \dfrac{-L_{yU}R_{armL}}{L_Z}I_{Ld2}\right)_{d2} + \\ \quad \left(\dfrac{-L_2}{L_Z}V_{Uq2} + \dfrac{-L_{yU}}{L_Z}V_{Lq2} + \dfrac{-L_2 R_{armU}}{L_Z}I_{Uq2} + \dfrac{-L_{yU}R_{armL}}{L_Z}I_{Lq2}\right)_{q2} \end{cases} \tag{16}$$

The second-harmonic expression of (2) and (3) can be given similarly as:

$$\begin{aligned} \left(-2\omega C_{armL}V_{Lq2}^{\Sigma}\right)_{d2} + &\left(2\omega C_{armL}V_{Ld2}^{\Sigma}\right)_{q2} = \\ &\left(\dfrac{M_{Ld}I_{Ld}}{2} - \dfrac{M_{Lq}I_{Lq}}{2} + M_{L0}I_{Ld2}\right)_{d2} + \\ &\left(\dfrac{M_{Lq}I_{Ld}}{2} + \dfrac{M_{Ld}I_{Lq}}{2} + M_{L0}I_{Lq2}\right)_{q2} \end{aligned} \tag{17}$$

$$\begin{aligned} \left(V_{Ld2}\right)_{d2} + \left(V_{Lq2}\right)_{q2} = &\left(\dfrac{M_{Ld}V_{Ld}^{\Sigma}}{2} - \dfrac{M_{Lq}V_{Lq}^{\Sigma}}{2} + M_{L0}V_{Ld2}^{\Sigma}\right)_{d2} + \\ &\left(\dfrac{M_{Lq}V_{Ld}^{\Sigma}}{2} + \dfrac{M_{Ld}V_{Lq}^{\Sigma}}{2} + M_{L0}V_{Lq2}^{\Sigma}\right)_{q2} \end{aligned} \tag{18}$$

E. SHCSC

The second-harmonic arm current can be eliminated by using feedback proportional integral (PI) control of I_{d2} and I_{q2}, which is similar to conventional AC/DC MMC [11]. SHCSC is considered as optional in this paper because the second-harmonic currents in NIMDC are low. The equations below show model modification when SHCSC is used. The modulation indices will include the second-harmonic terms as:

$$
\begin{cases}
m_U(t) = M_{U0} + M_U \cos(\omega t) + M_{U2} \cos\left(2\omega t + \phi_{m_{U2}}\right) = \\
\quad \left(M_{U0}\right)_0 + \left(M_U\right)_d + \left(M_{Ud2}\right)_{d2} + \left(M_{Uq2}\right)_{q2} \\
m_L(t) = M_{L0} + M_L \cos(\omega t + \phi_{m_L}) + M_{L2} \cos\left(2\omega t + \phi_{m_{L2}}\right) = \\
\quad \left(M_{L0}\right)_0 + \left(M_{Ld}\right)_d + \left(M_{Lq}\right)_q + \left(M_{Ld2}\right)_{d2} + \left(M_{Lq2}\right)_{q2}
\end{cases}
$$

(19)

where $\phi_{m_{U2}}$ and $\phi_{m_{L2}}$ are the phase shifts of the second-harmonic component of the upper-arm and lower-arm control signals, respectively.

It is assumed that the SHCSC suppresses perfectly the second-harmonic components of the arm currents, i. e., $I_{Ud2} = I_{Uq2} = I_{Ld2} = I_{Lq2} = 0$. Replacing this assumption in (16) yields $V_{Ud2} = V_{Uq2} = V_{Ld2} = V_{Lq2} = 0$. Equation (11) will be rewritten as:

$$
V_{L0} = M_{L0}V_{L0}^\Sigma + \frac{M_{Ld}V_{Ld}^\Sigma}{2} + \frac{M_{Lq}V_{Lq}^\Sigma}{2} + \frac{M_{Ld2}V_{Ld2}^\Sigma}{2} + \frac{M_{Lq2}V_{Lq2}^\Sigma}{2}
$$

(20)

Equations (14) and (15) are rewritten as:

$$
\left(-\omega C_{armL}V_{Lq}^\Sigma\right)_d + \left(\omega C_{armL}V_{Ld}^\Sigma\right)_q = \\
\left(M_{L0}I_{Ld} + M_{Ld}I_{L0} + \frac{M_{Ld2}I_{Ld}}{2} + \frac{M_{Lq2}I_{Lq}}{2}\right)_d + \\
\left(M_{L0}I_{Lq} + M_{Lq}I_{L0} - \frac{M_{Ld2}I_{Lq}}{2} + \frac{M_{Lq2}I_{Ld}}{2}\right)_q
$$

(21)

$$
\left(V_{Ld}\right)_d + \left(V_{Lq}\right)_q = \left(M_{Ld}V_{L0}^\Sigma + M_{L0}V_{Ld}^\Sigma + \frac{M_{Ld2}V_{Ld}^\Sigma}{2} + \frac{M_{Lq2}V_{Lq}^\Sigma}{2} + \right. \\
\left. \frac{M_{Ld2}V_{Ld}^\Sigma}{2} + \frac{M_{Lq2}V_{Lq}^\Sigma}{2}\right)_d + \left(M_{Lq}V_{L0}^\Sigma + M_{L0}V_{Lq}^\Sigma - \frac{M_{Lq}V_{Ld2}^\Sigma}{2} + \right. \\
\left. \frac{M_{Ld}V_{Lq2}^\Sigma}{2} + \frac{M_{Lq2}V_{Ld}^\Sigma}{2} - \frac{M_{Ld2}V_{Lq}^\Sigma}{2}\right)_q
$$

(22)

The second-harmonic arm sum voltages in (17) are rewritten as:

$$
\left(-2\omega C_{armL}V_{Lq2}^\Sigma\right)_{d2} + \left(2\omega C_{armL}V_{Ld2}^\Sigma\right)_{q2} = \\
\left(\frac{M_{Ld}I_{Ld}}{2} - \frac{M_{Lq}I_{Lq}}{2} + M_{Ld2}I_{L0}\right)_{d2} + \\
\left(\frac{M_{Lq}I_{Ld}}{2} + \frac{M_{Ld}I_{Lq}}{2} + M_{Lq2}I_{L0}\right)_{q2}
$$

(23)

By similarly rewriting (18) and considering $V_{Ud2} = V_{Uq2} = V_{Ld2} = V_{Lq2} = 0$, the required $d2q2$ components of the lower-arm modulation signals can be obtained as:

$$
\begin{cases}
M_{Ld2} = \dfrac{-M_{Ld}V_{Ld}^\Sigma}{2V_{L0}^\Sigma} + \dfrac{M_{Lq}V_{Lq}^\Sigma}{2V_{L0}^\Sigma} - \dfrac{M_{L0}V_{Ld2}^\Sigma}{V_{L0}^\Sigma} \\
M_{Lq2} = \dfrac{-M_{Lq}V_{Ld}^\Sigma}{2V_{L0}^\Sigma} - \dfrac{M_{Ld}V_{Lq}^\Sigma}{2V_{L0}^\Sigma} - \dfrac{M_{L0}V_{Lq2}^\Sigma}{V_{L0}^\Sigma}
\end{cases}
$$

(24)

IV. NIMDC Phasor Model

A. Non-linear Open-loop Model

Equations (9)-(18) in the 3 coordinate frames can be combined to obtain a single-phasor model as (25), which contains multiple non-linear terms caused by the multiplication with the control signals in matrix form.

$$
Ax = u + Bv
$$

(25)

where x is the vector of variables; u is the vector of all non-linear terms; and v is the vector of external signals (disturbances). The model is expanded (including both the upper- and lower-arm equations) and presented in matrix form in Appendix A. The matrix form of the model with SHCSC can be presented in a similar way.

B. Controller Model

The NIMDC without SHCSC has 5 control signals, which are M_{U0}, M_{Ud}, M_{L0}, M_{Ld}, and M_{Lq}, as shown in (5). There are numerous options for control strategy, and a generic control is assumed, as shown in Fig. 2 [10].
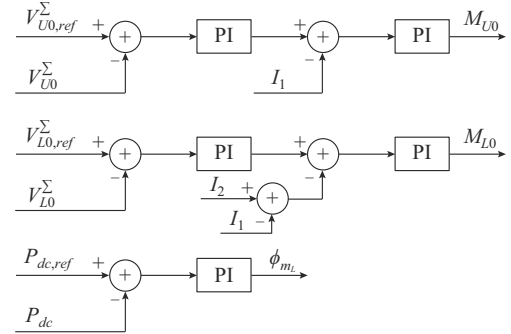
Fig. 2. Block diagram of NIMDC control.

The zero-sequence signals M_{U0} and M_{L0} are employed to regulate arm sum voltages, which ensures energy balancing in the converter arms. The inner current control is used to improve system response and to limit the current in case of disturbances. The DC power flow P_{dc} is regulated at the reference DC power $P_{dc,ref}$ by using the phase shift ϕ_{m_L} between the control signals of the lower and upper arms.

One good approach to selecting the magnitude of fundamental-frequency component control (M_U and M_L) is to maximize the AC voltage ($M_{U0} + M_U \leq 1$), in order to minimize the losses:

$$
\begin{cases}
M_U = M_L = \min\left(M_{U0}, M_{L0}\right) \\
M_{Ld} = M_L \cos\phi_{m_L} \\
M_{Lq} = M_L \sin\phi_{m_L} \\
M_{Ud} = M_U
\end{cases}
$$

(26)

C. Estimation of Control Signals

The control signals can be determined using numerical iterative methods, which are time-consuming. To avoid iterations, this paper shows that for this converter, it is possible to obtain accurate explicit linear model by estimating the control signals. This estimation can be achieved if the following assumptions are made.

1) Ripples of upper- and lower-arm sum voltages are usually small and can be ignored, i.e., dq and $d2q2$ components are zero and $v_{armU}^{\Sigma}(t) \approx V_{U0}^{\Sigma} = V_{U0,ref}^{\Sigma}$, $v_{armL}^{\Sigma}(t) \approx V_{L0}^{\Sigma} = V_{L0,ref}^{\Sigma}$.

2) $V_{Uq} \approx 0$ since fundamental voltage follows the control signal which is aligned with the coordinate frame.

3) The phase angle of lower-arm control signal ϕ_{m_L} is approximated by an average of phase angles of the upper- and lower-arm voltages.

From (11) and considering the assumption 1, the zero-sequence components of the arm voltage are estimated as $V_{U0} \approx M_{U0} V_{U0,ref}^{\Sigma}$, $V_{U0} \approx M_{U0} V_{L0,ref}^{\Sigma}$ and by replacing these estimations in (9), the zero-sequence components of the control signals are approximated as:

$$\begin{cases} M_{U0} \approx \dfrac{V_1 - V_2 - R_{armU} I_{U0}}{V_{U0,ref}^{\Sigma}} \\ M_{L0} \approx \dfrac{V_2 - R_{armL} I_{L0}}{V_{L0,ref}^{\Sigma}} \end{cases} \quad (27)$$

where $I_{U0} = I_1/3$; and $I_{L0} = (I_1 - I_2)/3$.

The arm DC power must be equal to the arm AC power in one cycle to maintain power balance. This condition for the upper arm of converter considering assumption 2 yields:

$$\left(V_1 - V_2\right)\frac{I_1}{3} \approx 0.5 V_{Ud} I_{Ud} \quad (28)$$

V_{Ud} and I_{Ud} can be respectively estimated from (15) and the first equation of (13) by considering assumptions 1 and 2 and assuming the lossless converter as:

$$\begin{cases} V_{Ud} \approx M_U V_{U0,ref}^{\Sigma} \\ I_{Ud} \approx \dfrac{-L_2}{\omega L_Z} V_{Lq} \end{cases} \quad (29)$$

By replacing (29) in (28) and considering $P = P_{dc,ref} = V_1 I_1$, V_{Lq} is approximated as:

$$V_{Lq} \approx \frac{-2\omega L_Z}{L_2 M_U V_{U0,ref}^{\Sigma}} \left(V_1 - V_2\right) \frac{P_{dc,ref}}{3V_1} \quad (30)$$

Using (30) and assumption 3, and considering that the amplitude of the upper- and lower-arm fundamental voltages are the same, i.e., $V_L \approx V_U \approx V_{Ud} \approx M_U V_{U0,ref}^{\Sigma}$, the phase angle of the lower-arm control signal is then estimated as:

$$\phi_{m_L} \approx 0.5 \arcsin\left(\frac{V_{Lq}}{V_L}\right) \approx 0.5 \arcsin\left(\frac{-2\omega L_Z \left(V_1 - V_2\right) P_{dc,ref}}{3 L_2 V_1 \left(M_U V_{U0,ref}^{\Sigma}\right)^2}\right) \quad (31)$$

Using (26), (27), and (31), the 5 control signals can be determined.

D. Structure of Closed-loop Linear Model

By replacing the estimated control signals in (25), a closed-loop phasor model is obtained. The closed-loop model can then be linearized and presented as $\boldsymbol{A}_{CL}\boldsymbol{x} = \boldsymbol{Bv}$, where the matrices can be obtained using linearization; and $\boldsymbol{A}_{CL}$ is the matrix of the closed-loop linear phasor model .

Figure 3 shows the proposed phasor model structure. The model calculates explicitly all the NIMDC zero-sequence, fundamental-frequency, and second-harmonic variables for upper and lower arms.
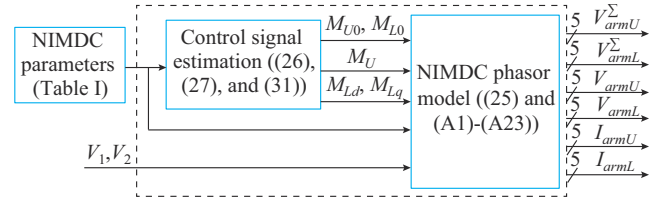

Fig. 3.   Proposed phasor model structure.

V. PHASOR MODEL VERIFICATION

A. PSCAD Test Model

The PSCAD test model of the system includes a 3-phase NIMDC connected to a DC source at each side, following CIGRE B4.76 approach [6]. Each arm valve is represented using an improved average non-linear MMC model which has been verified for a wide range of operating conditions in [19]. The time step of PSCAD simulation is reduced to 1 μs to increase the accuracy.

The proposed phasor model is verified against the PSCAD model using 3 test cases given in Table I. The test cases are purposely developed with widely different voltage ratios, ratings (parameters), operating frequencies, and power flows to examine model robustness. The upper- and lower-arm capacitance and inductance of NIMDC and the inductances of L_2 are selected to keep the voltage ripple of cell capacitance around ±5% at the rated power. The reference arm sum voltages are $V_{U0,ref}^{\Sigma} = V_{L0,ref}^{\Sigma} = V_1 = 320$ kV, and the number of cells is selected as $N_U = N_L = 160$ for all test cases to keep the cell rated voltage of 2 kV. The equivalent upper- and lower-arm resistances are 1.44 Ω and 0.96 Ω, respectively, for all test cases.

TABLE I
NIMDC PARAMETERS FOR 3 TEST CASES

Case	P_{rated} (MW)	$P_{dc,ref}$ (p.u.)	V_{dc} (kV)	Frequency (Hz)	C_{sm} (μF)	L_{arm} (mH)	L_2 (mH)
1	600	1	$V_1 = 320$, $V_2 = 250$	150	$C_{smU} = 2400$, $C_{smL} = 13200$	$L_{armU} = 11$, $L_{armL} = 11$	80
2	600	−0.5	$V_1 = 320$, $V_2 = 160$	200	$C_{smU} = 6800$, $C_{smL} = 6800$	$L_{armU} = 8$, $L_{armL} = 8$	60
3	300	0.2	$V_1 = 320$, $V_2 = 80$	300	$C_{smU} = 8400$, $C_{smL} = 2050$	$L_{armU} = 7$, $L_{armL} = 5$	40

B. Verification of Open-loop Model

The quantitative comparison results for all 30 variables of the model for test case 1 are given in Table II. All the zero-sequence, fundamental-frequency, and second-harmonic dq

variables show good matching, which implies that modelling up to the second harmonic gives very high accuracy, and higher harmonics would not be required.

TABLE II
VERIFICATION RESULT FOR TEST CASE 1

| Variable | Type | Magnitude of different components | | | | | Norm-2 error (%) |
		Zero sequence	d	q	d2	q2	
V_{armU}^{Σ}	PSCAD	320.000	1.417	9.110	0.504	4.810	0.035
	Model	320.000	1.319	9.120	0.502	4.770	
V_{armL}^{Σ}	PSCAD	320.000	−8.360	13.320	0.526	−1.170	0.024
	Model	320.000	−8.430	13.310	0.525	−1.154	
V_{armU}	PSCAD	69.100	70.400	2.490	0.270	2.040	0.060
	Model	69.100	70.300	2.490	0.253	2.020	
V_{armL}	PSCAD	250.200	−75.000	25.300	1.002	−2.570	0.034
	Model	250.200	−75.100	25.300	1.002	−2.520	
I_{armU}	PSCAD	0.629	−1.239	0.077	0.004	0.030	0.413
	Model	0.628	−1.238	0.072	0.003	0.030	
I_{armL}	PSCAD	−0.165	−1.374	−0.823	0.018	0.032	0.317
	Model	−0.164	−1.374	−0.828	0.017	0.032	

The norm-2 error for each variable x, $\|e_x\|$, is calculated as:

$$\|e_x\| = \frac{\|x_{PSCAD} - x_{Model}\|}{\|x_{PSCAD}\|} \times 100\% \quad (32)$$

where $x = [x_0, x_d, x_q, x_{d2}, x_{q2}]$. It is observed that the norm-2 errors are well below 0.5% for all variables。

Figure 4 shows the steady-state upper-arm sum voltage and arm current of PSCAD, and the reconstructed signals from the model output for test case 1 while Fig. 5 shows the steady-state error of upper-arm sum voltage and arm current. The reconstructed signals are generated based on (6) and (7), and the verification results for test case 1 are given in Table II. It is observed that the errors are very low.
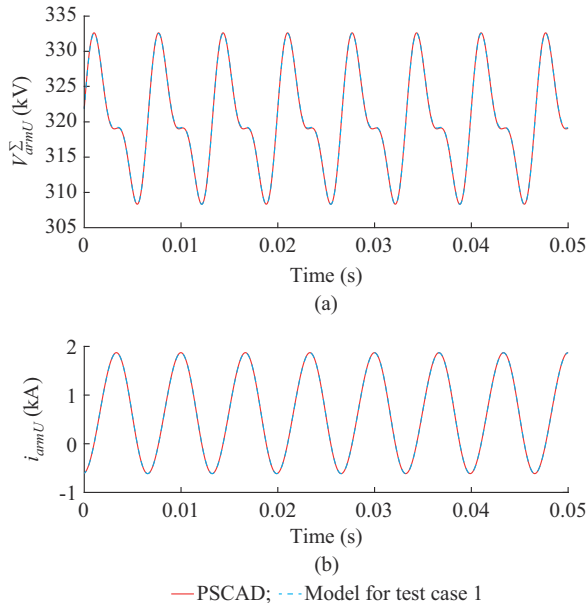

Fig. 4. Steady-state upper-arm sum voltage V_{armU}^{Σ} and arm current i_{armU}.
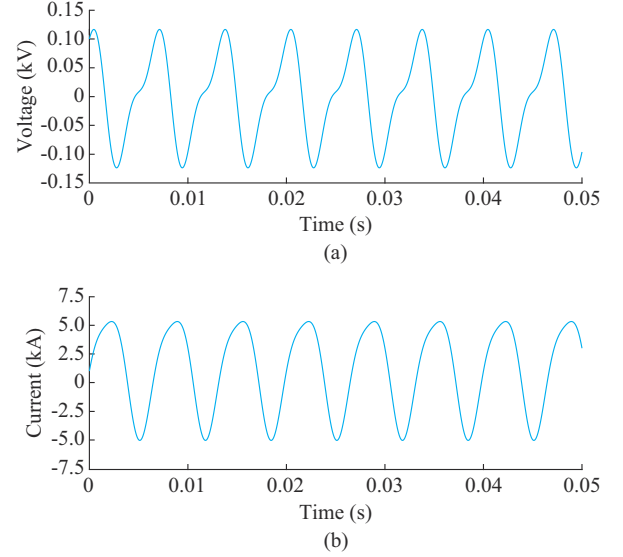

Fig. 5. Steady-state error of upper-arm sum voltage and arm current.

The verification results for test case 2 are provided in Table III. This illustrates that the model is accurate with different voltage ratios, operating frequencies, valve parameters, and power flows. The results also show that the magnitude of second harmonic is generally small compared with the conventional MMC AC/DC converter (around 2.5% of the fundamental frequency for test case 1, 30% for test case 2, and 8% for test case 3), and NIMDC may or may not need SHCSC.

TABLE III
VERIFICATION RESULT FOR TEST CASE 2

| Variable | Type | Magnitude of different components | | | | | Norm-2 error (%) |
		Zero sequence	d	q	d2	q2	
V_{armU}^{Σ}	PSCAD	320.000	12.340	−2.600	3.930	−1.324	0.048
	Model	319.900	12.330	−2.610	3.860	−1.320	
V_{armL}^{Σ}	PSCAD	320.000	−8.880	−3.460	2.830	1.905	0.022
	Model	320.000	−8.830	−3.460	2.790	1.896	
V_{armU}	PSCAD	160.500	167.100	−1.593	5.120	−1.295	0.089
	Model	160.400	167.000	−1.613	4.980	−1.301	
V_{armL}	PSCAD	159.700	−164.600	−12.470	3.770	1.970	0.121
	Model	159.700	−164.500	−12.470	3.520	1.938	
I_{armU}	PSCAD	−0.310	0.609	1.232	−0.025	0.221	0.663
	Model	−0.310	0.610	1.230	−0.024	0.212	
I_{armL}	PSCAD	0.323	0.693	−0.831	−0.035	0.217	0.860
	Model	0.324	0.694	−0.832	−0.033	0.208	

C. Verification of Closed-loop Model

Table IV shows the estimated control signal, using (26), (27), and (31) for test case 1 against those in the benchmark PSCAD model (obtained using the PI controllers of Fig. 2), and Table V gives the verification results of the closed-loop model with estimated control signals for test case 1.

It is observed that the control signal estimations are reasonably good, while the errors of the closed-loop model are

higher because of the assumptions in the control signal estimation. However, the accuracy is still adequate for most practical studies.

TABLE IV
ESTIMATED CONTROL SIGNAL FOR TEST CASE 1

Type	M_{U0}	M_{L0}	M_U	M_{Ld}	M_{Lq}
PSCAD	0.2155	0.7780	0.2188	−0.2139	0.0463
Phasor model	0.2159	0.7818	0.2188	−0.2114	0.0442

TABLE V
VERIFICATION RESULTS OF CLOSED-LOOP MODEL WITH ESTIMATED CONTROL SIGNAL FOR TEST CASE 1

Variable	Type	Magnitude of different components					Norm-2 error (%)
		Zero sequence	d	q	$d2$	$q2$	
V_{armU}^{Σ}	PSCAD	320.000	1.417	9.110	0.504	4.810	0.199
	Model	319.400	1.528	9.090	0.553	4.540	
V_{armL}^{Σ}	PSCAD	320.000	−8.360	13.320	0.526	−1.170	0.490
	Model	318.500	−8.190	12.880	0.518	−1.090	
V_{armU}	PSCAD	69.100	70.400	2.490	0.270	2.040	1.052
	Model	69.100	69.400	2.450	0.285	1.961	
V_{armL}	PSCAD	250.200	−75.000	25.300	1.002	−2.570	0.606
	Model	250.100	−73.800	24.200	0.985	−2.390	
I_{armU}	PSCAD	0.629	−1.239	0.077	0.004	0.030	4.170
	Model	0.596	−1.192	0.085	0.002	0.030	
I_{armL}	PSCAD	−0.165	−1.374	−0.823	0.018	0.032	3.570
	Model	−0.156	−1.321	−0.800	0.015	0.032	

D. Impact of Second Harmonic on Model Accuracy

A simplified model is obtained by equating the second-order harmonic of the variables ($d2$ and $q2$ components of V_{arm}^{Σ}, V_{arm}, and I_{arm}) in vectors $\boldsymbol{x}$ and $\boldsymbol{u}$, and matrix $\boldsymbol{A}$ in (A1) and (A2) to zero, which reduces the number of variables from 30 to 18.

The accuracy of this reduced-order open-loop model for test case 3 is compared with that for both the PSCAD and full-order models, and the verification results are shown in Table VI.

It is observed that the simplified model errors are much higher for almost all variables. This implies that the second harmonic has significant impact on the model accuracy, and the reduced phasor modelling with only two coordinate frames (0 and dq) [12] may not be accurate enough for many applications. This is in agreement with conclusions from [2] that second harmonic affects power flow. Such a reduced model might be beneficial only in specific cases where processing resources are limited, and a lower accuracy is acceptable.

E. Verification of Phasor Model with SHCSC

The phasor model with SHCSC is also verified, and the verification results for test case 1 are given in Table VII. It is observed that the matching in test case 1 is better than in

the case without SHCSC. Table VIII shows that the magnitude of the second-harmonic control signals is small and the matching with PSCAD model is excellent. It is also concluded that $d2q2$ coordinate frame modelling should be used even when SHCSC is employed, since arm sum voltages contain second harmonic and there is a coupling with dq frame and power flow, as shown in Table VII.

TABLE VI
VERIFICATION OF REDUCED- AND FULL-ORDER PHASOR MODELS (TEST CASE 3)

Variable	Type	Magnitude of different components					Norm-2 error (%)
		Zero sequence	d	q	$d2$	$q2$	
V_{armU}^{Σ}	PSCAD	320.000	3.270	2.670	0.429	0.238	
	Full-order	320.000	3.260	2.670	0.425	0.241	0.007
	Reduced-order	320.000	3.290	2.620			0.154
V_{armL}^{Σ}	PSCAD	320.000	−6.420	2.310	1.678	−1.190	
	Full-order	319.700	−6.410	2.290	1.665	−1.172	0.090
	Reduced-order	319.900	−6.060	2.240			0.654
V_{armU}	PSCAD	239.900	82.500	2.040	0.731	0.512	
	Full-order	239.900	82.500	2.030	0.726	0.514	0.006
	Reduced-order	239.900	82.500	1.960			0.354
V_{armL}	PSCAD	80.200	−81.500	6.840	1.250	−0.660	
	Full-order	80.200	−81.500	6.680	1.191	−0.636	0.155
	Reduced-order	80.200	−81.200	6.540			1.281
I_{armU}	PSCAD	0.063	−0.375	0.424	−0.001	0.043	
	Full-order	0.063	−0.374	0.424	−0.001	0.041	0.329
	Reduced-order	0.061	−0.366	0.435			7.910
I_{armL}	PSCAD	−0.182	−0.407	−0.589	0.003	0.045	
	Full-order	−0.181	−0.405	−0.588	0.003	0.044	0.376
	Reduced-order	−0.177	−0.396	−0.576			6.540

TABLE VII
VERIFICATION OF PHASOR MODEL WITH SHCSC (TEST CASE 1)

Variable	Type	Magnitude of different components					Norm-2 error (%)
		Zero sequence	d	q	$d2$	$q2$	
V_{armU}^{Σ}	PSCAD	320.000	1.443	9.140	0.136	4.840	0.020
	Model	320.000	1.390	9.160	0.140	4.810	
V_{armL}^{Σ}	PSCAD	320.000	−8.400	13.330	0.355	−1.081	0.014
	Model	320.000	−8.440	13.330	0.354	−1.072	
V_{armU}	PSCAD	69.100	70.300	2.510	0.009	−0.036	0.043
	Model	69.100	70.300	2.500	0	0	
V_{armL}	PSCAD	250.200	−74.900	25.300	−0.010	−0.037	0.023
	Model	250.200	−75.000	25.300	0	0	
I_{armU}	PSCAD	0.629	−1.238	0.076	0	0	0.255
	Model	0.630	−1.240	0.073	0	0	
I_{armL}	PSCAD	−0.164	−1.377	−0.823	0	0	0.179
	Model	−0.165	−1.376	−0.826	0	0	

VI. DEMONSTRATION OF PHASOR MODEL APPLICATIONS

A. Impact of NIMDC Parameters on Ripple

The proposed phasor model can be used to study the impact of the NIMDC parameters on the performance and for the converter design purposes.

Figure 6 shows the voltage ripple of capacitors versus the lower-arm cell capacitance for three different arm inductances while all other parameters are kept constant as in the test case 1. It shows that both upper- and lower-arm cell voltage ripples decrease nonlinearly by increasing the lower-arm capacitance even though upper-arm capacitance is constant ($C_{smU} = 2400$ µF). It also shows that the arm inductance affects the voltage ripples in a complex and non-linear manner. Such multidimensional design problems are challenging on time-domain simulators.

TABLE VIII
VERIFICATION OF SECOND-HARMONIC CONTROL SIGNALS FOR TEST CASE 1 WITH SHCSC

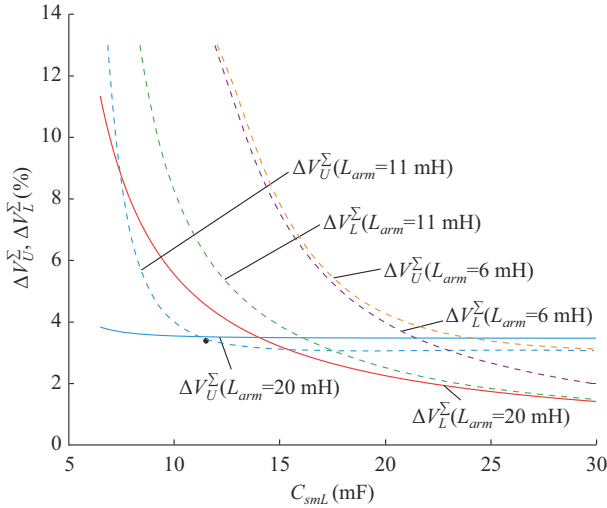| Type	M_{Ud2}	M_{Uq2}	M_{Ld2}	M_{Lq2}
PSCAD	−0.0006	−0.0064	−0.0027	0.0078
Model	−0.0006	−0.0064	−0.0027	0.0077

Fig. 6. Upper- and lower-arm sum voltage ripples versus lower-arm SM capacitance (test case 1).

The voltage ripple is considered as the sum of fundamental frequency and second harmonic on the arm sum voltage as below:

$$\begin{cases} \Delta V_{armU}^{\Sigma} = \sqrt{\left(V_{Ud}^{\Sigma}\right)^2 + \left(V_{Uq}^{\Sigma}\right)^2 + \left(V_{Ud2}^{\Sigma}\right)^2 + \left(V_{Uq2}^{\Sigma}\right)^2} \\ \Delta V_{armL}^{\Sigma} = \sqrt{\left(V_{Ld}^{\Sigma}\right)^2 + \left(V_{Lq}^{\Sigma}\right)^2 + \left(V_{Ld2}^{\Sigma}\right)^2 + \left(V_{Lq2}^{\Sigma}\right)^2} \end{cases} \quad (33)$$

B. Eigenvalue Stability Analysis

The stability of the NIMDC for test case 1 has been analysed using the eigenvalues of A_{CL}. With the design parameters, all the eigenvalues are in the left half plane, implying that the system is stable with the dominant eigenvalues of $-0.2362 \pm j0.0555$.

The system eigenvalues move toward the right half plane (the instability region) by decreasing the main parameters of each converter, i.e., L_{arm}, L_2, C_{armU}, C_{armL}, and the operating frequency. Comparing the phasor and PSCAD models, Table IX shows the minimum value for each NIMDC parameter of stable operating for test case 1 and summarizes the theoretical stability limit for each parameter while other parameters are kept unchanged. There is no theoretical limit for L_2 based on the model.

TABLE IX
THE MINIMUM VALUE FOR EACH NIMDC PARAMETER OF STABLE OPERATING FOR TEST CASE 1

Type	L_{arm} (mH)	L_2 (mH)	C_{armU} (µF)	C_{armL} (µF)	Frequency (Hz)
Model	5		485	5600	102
PSCAD	7	2	1100	6850	121

It is observed that the stability limits based on the phasor model are more optimistic than the corresponding limits in PSCAD. Since phasor model is valid only in steady state, the PSCAD results indicate the dynamic stability limits. It should be noted that phasor models are not usually suitable for stability analysis.

VII. CONCLUSION

The accurate 30th-order open-loop phasor model for high-power NIMDC is proposed. It is concluded that the model should consider the converter variables in zero sequence, the rotating dq frame at the fundamental frequency, and the $d2q2$ frame at double the fundamental frequency. The model is convenient for power flow studies, as it includes the external DC voltages and the control signals as the external inputs. It is demonstrated that $d2q2$ coordinate frame is important, since there is a significant coupling among the zero-sequence, fundamental frequency, and second-harmonic variables in the non-linear model. A linearized closed-loop phasor model is also developed by estimating the control signals which is suitable for linear system studies. A thorough verification of the proposed model against benchmark PSCAD model is performed for 3 test cases with different voltage step ratios, power flows, and operating frequencies, and the observed accuracy is found to be very good. As a demonstration of the proposed model, the study of lower-arm cell capacitance demonstrates significant cross coupling between the upper- and lower-arms variables including harmonics. In addition, the model is used to determine eigenvalues and to perform basic stability analysis.

APPENDIX A

The vectors and matrices of the proposed NIMDC phasor model (25) are as below:

$$\begin{cases} \boldsymbol{x} = \begin{bmatrix} V_{armU}^{\Sigma} & V_{armL}^{\Sigma} & V_{armU} & V_{armL} & I_{armU} & I_{armL} \end{bmatrix}_{30 \times 1}^{T} \\ \boldsymbol{V}_{armU}^{\Sigma} = \begin{bmatrix} V_{U0}^{\Sigma} & V_{Ud}^{\Sigma} & V_{Uq}^{\Sigma} & V_{Ud2}^{\Sigma} & V_{Uq2}^{\Sigma} \end{bmatrix}^{T} \\ \boldsymbol{V}_{armL}^{\Sigma} = \begin{bmatrix} V_{L0}^{\Sigma} & V_{Ld}^{\Sigma} & V_{Lq}^{\Sigma} & V_{Ld2}^{\Sigma} & V_{Lq2}^{\Sigma} \end{bmatrix}^{T} \\ \boldsymbol{V}_{armU} = \begin{bmatrix} V_{U0} & V_{Ud} & V_{Uq} & V_{Ud2} & V_{Uq2} \end{bmatrix}^{T} \\ \boldsymbol{V}_{armL} = \begin{bmatrix} V_{L0} & V_{Ld} & V_{Lq} & V_{Ld2} & V_{Lq2} \end{bmatrix}^{T} \\ \boldsymbol{I}_{armU} = \begin{bmatrix} I_{U0} & I_{Ud} & I_{Uq} & I_{Ud2} & I_{Uq2} \end{bmatrix}^{T} \\ \boldsymbol{I}_{armL} = \begin{bmatrix} I_{L0} & I_{Ld} & I_{Lq} & I_{Ld2} & I_{Lq2} \end{bmatrix}^{T} \end{cases} \tag{A1}$$

$$\boldsymbol{A} = \begin{bmatrix} \boldsymbol{I}_{5\times5} & \boldsymbol{0}_{5\times5} & \boldsymbol{0}_{5\times5} & \boldsymbol{0}_{5\times5} & \boldsymbol{0}_{5\times5} & \boldsymbol{0}_{5\times5} \\ \boldsymbol{0}_{5\times5} & \boldsymbol{I}_{5\times5} & \boldsymbol{0}_{5\times5} & \boldsymbol{0}_{5\times5} & \boldsymbol{0}_{5\times5} & \boldsymbol{0}_{5\times5} \\ \boldsymbol{0}_{5\times5} & \boldsymbol{0}_{5\times5} & \boldsymbol{I}_{5\times5} & \boldsymbol{0}_{5\times5} & \boldsymbol{A}_{35} & \boldsymbol{0}_{5\times5} \\ \boldsymbol{0}_{5\times5} & \boldsymbol{0}_{5\times5} & \boldsymbol{0}_{5\times5} & \boldsymbol{I}_{5\times5} & \boldsymbol{0}_{5\times5} & \boldsymbol{A}_{46} \\ \boldsymbol{0}_{5\times5} & \boldsymbol{0}_{5\times5} & \boldsymbol{A}_{53} & \boldsymbol{A}_{54} & \boldsymbol{I}_{5\times5}+\boldsymbol{A}_{55} & \boldsymbol{A}_{56} \\ \boldsymbol{0}_{5\times5} & \boldsymbol{0}_{5\times5} & \boldsymbol{A}_{63} & \boldsymbol{A}_{64} & \boldsymbol{A}_{65} & \boldsymbol{I}_{5\times5}+\boldsymbol{A}_{66} \end{bmatrix} \tag{A2}$$

$$\boldsymbol{A}_{35} = R_{armU}\boldsymbol{A}_{V} \tag{A3}$$

$$\boldsymbol{A}_{46} = R_{armL}\boldsymbol{A}_{V} \tag{A4}$$

$$\boldsymbol{A}_{53} = \frac{L_{yL}}{\omega L_{Z}}\boldsymbol{A}_{I} \tag{A5}$$

$$\boldsymbol{A}_{54} = \frac{L_{2}}{\omega L_{Z}}\boldsymbol{A}_{I} \tag{A6}$$

$$\boldsymbol{A}_{55} = \frac{L_{yL}R_{armU}}{\omega L_{Z}}\boldsymbol{A}_{I} \tag{A7}$$

$$\boldsymbol{A}_{56} = \frac{L_{2}R_{armL}}{\omega L_{Z}}\boldsymbol{A}_{I} \tag{A8}$$

$$\boldsymbol{A}_{63} = \frac{L_{2}}{\omega L_{Z}}\boldsymbol{A}_{I} \tag{A9}$$

$$\boldsymbol{A}_{64} = \frac{L_{yU}}{\omega L_{Z}}\boldsymbol{A}_{I} \tag{A10}$$

$$\boldsymbol{A}_{65} = \frac{L_{2}R_{armU}}{\omega L_{Z}}\boldsymbol{A}_{I} \tag{A11}$$

$$\boldsymbol{A}_{66} = \frac{L_{yU}R_{armL}}{\omega L_{Z}}\boldsymbol{A}_{I} \tag{A12}$$

$$\boldsymbol{A}_{V} = \begin{bmatrix} 1 & 0 & 0 & 0 & 0 \\ 0 & 0 & 0 & 0 & 0 \\ 0 & 0 & 0 & 0 & 0 \\ 0 & 0 & 0 & 0 & 0 \\ 0 & 0 & 0 & 0 & 0 \end{bmatrix} \tag{A13}$$

$$\boldsymbol{A}_{I} = \begin{bmatrix} 0 & 0 & 0 & 0 & 0 \\ 0 & 0 & 1 & 0 & 0 \\ 0 & -1 & 0 & 0 & 0 \\ 0 & 0 & 0 & 0 & 0.5 \\ 0 & 0 & 0 & -0.5 & 0 \end{bmatrix} \tag{A14}$$

$$\boldsymbol{B} = \begin{bmatrix} \boldsymbol{0}_{10\times1} & \boldsymbol{0}_{10\times1} \\ \hline 1 & -1 \\ \hline \boldsymbol{0}_{4\times1} & \boldsymbol{0}_{4\times1} \\ \hline 0 & 1 \\ \hline \boldsymbol{0}_{14\times1} & \boldsymbol{0}_{14\times1} \end{bmatrix} \tag{A15}$$

$$\boldsymbol{v} = \begin{bmatrix} V_{1} & V_{2} \end{bmatrix}^{T} \tag{A16}$$

$$\boldsymbol{u} = \begin{bmatrix} u_{1} & u_{2} & u_{3} & u_{4} & u_{5} & u_{6} \end{bmatrix}^{T} \tag{A17}$$

$$\boldsymbol{u}_{1} = \begin{bmatrix} \dfrac{V_{U0}}{M_{U0}} - \dfrac{M_{U}V_{Ud}^{\Sigma}}{2M_{U0}} \\[2ex] \dfrac{M_{U0}I_{Uq}}{\omega C_{armU}} + \dfrac{M_{U}I_{Uq2}}{2\omega C_{armU}} \\[2ex] \dfrac{-I_{U0}M_{U}}{\omega C_{armU}} - \dfrac{M_{U0}I_{Ud}}{\omega C_{armU}} - \dfrac{M_{U}I_{Ud2}}{2\omega C_{armU}} \\[2ex] \dfrac{M_{U}I_{Uq}}{4\omega C_{armU}} + \dfrac{M_{U0}I_{Uq2}}{2\omega C_{armU}} \\[2ex] \dfrac{-M_{U}I_{Ud}}{4\omega C_{armU}} - \dfrac{M_{U0}I_{Ud2}}{2\omega C_{armU}} \end{bmatrix} \tag{A18}$$

$$\boldsymbol{u}_{2} = \begin{bmatrix} \dfrac{V_{L0}}{M_{L0}} - \dfrac{M_{Ld}V_{Ld}^{\Sigma}}{2M_{L0}} - \dfrac{M_{Lq}V_{Lq}^{\Sigma}}{2M_{L0}} \\[2ex] \dfrac{I_{L0}M_{Lq}}{\omega C_{armL}} + \dfrac{M_{L0}I_{Lq}}{\omega C_{armL}} - \dfrac{M_{Lq}I_{Ld2}}{2\omega C_{armL}} + \dfrac{M_{Ld}I_{Lq2}}{2\omega C_{armL}} \\[2ex] \dfrac{-I_{L0}M_{Ld}}{\omega C_{armL}} - \dfrac{M_{L0}I_{Ld}}{\omega C_{armL}} - \dfrac{M_{Ld}I_{Ld2}}{2\omega C_{armL}} - \dfrac{M_{Lq}I_{Lq2}}{2\omega C_{armL}} \\[2ex] \dfrac{M_{Lq}I_{Ld}}{4\omega C_{armL}} + \dfrac{M_{Ld}I_{Lq}}{4\omega C_{armL}} + \dfrac{M_{L0}I_{Lq2}}{2\omega C_{armL}} \\[2ex] \dfrac{-M_{Ld}I_{Ld}}{4\omega C_{armL}} + \dfrac{M_{Lq}I_{Lq}}{4\omega C_{armL}} - \dfrac{M_{L0}I_{Ld2}}{2\omega C_{armL}} \end{bmatrix} \tag{A19}$$

$$\boldsymbol{u}_{3} = \begin{bmatrix} 0 \\[2ex] M_{U}V_{U0}^{\Sigma} + M_{U0}V_{Ud}^{\Sigma} + \dfrac{M_{U}V_{Ud2}^{\Sigma}}{2} \\[2ex] M_{U0}V_{Uq}^{\Sigma} + \dfrac{M_{U}V_{Uq2}^{\Sigma}}{2} \\[2ex] \dfrac{M_{U}V_{Ud}^{\Sigma}}{2} + M_{U0}V_{Ud2}^{\Sigma} \\[2ex] \dfrac{M_{U}V_{Uq}^{\Sigma}}{2} + M_{U0}V_{Uq2}^{\Sigma} \end{bmatrix} \tag{A20}$$

$$\boldsymbol{u}_6 = \begin{bmatrix} -\dfrac{M_{Ld}I_{Ld}}{2M_{L0}} - \dfrac{M_{Lq}I_{Lq}}{2M_{L0}} & 0 & 0 & 0 & 0 \end{bmatrix}^{\mathrm{T}} \quad (A21)$$

$$\boldsymbol{u}_4 = \begin{bmatrix} 0 \\ M_{Ld}V_{L0}^{\Sigma} + M_{L0}V_{Ld}^{\Sigma} + \dfrac{M_{Ld}V_{Ld2}^{\Sigma}}{2} + \dfrac{M_{Lq}V_{Lq2}^{\Sigma}}{2} \\ M_{Lq}V_{L0}^{\Sigma} + M_{L0}V_{Lq}^{\Sigma} - \dfrac{M_{Lq}V_{Ld2}^{\Sigma}}{2} + \dfrac{M_{Ld}V_{Lq2}^{\Sigma}}{2} \\ \dfrac{M_{Ld}V_{Ld}^{\Sigma}}{2} - \dfrac{M_{Lq}V_{Lq}^{\Sigma}}{2} + M_{L0}V_{Ld2}^{\Sigma} \\ \dfrac{M_{Lq}V_{Ld}^{\Sigma}}{2} + \dfrac{M_{Ld}V_{Lq}^{\Sigma}}{2} + M_{L0}V_{Lq2}^{\Sigma} \end{bmatrix} \quad (A22)$$

$$\boldsymbol{u}_5 = \begin{bmatrix} -\dfrac{M_{U}I_{Ud}}{2M_{U0}} & 0 & 0 & 0 & 0 \end{bmatrix}^{\mathrm{T}} \quad (A23)$$

REFERENCES

[1] M. Wang, T. An, H. Ergun *et al.*, "Review and outlook of HVDC grids as backbone of transmission system," *CSEE Journal of Power and Energy Systems*, vol. 7, no. 4, pp. 797-810, Jul. 2021.

[2] D. Jovcic, *High Voltage Direct Current Transmission: Converters Systems and DC Grids*. New York: Wiley, 2019.

[3] A. Mokhberdoran, J. Sau-Bassols, E. Prieto-Araujo *et al.*, "Fault mode operation strategies for dual H-bridge current flow controller in meshed HVDC grid," *Electric Power Systems Research*, vol. 190, pp. 163-172, Mar. 2018.

[4] CIGRE WG B4.52, "HVDC grid feasibility study," Paris, Tech. Rep. CIGRE technical brochure 533, Apr. 2013.

[5] CIGRE WG B4.58, "Control methodlogies for direct voltage and power flow in meshed HVDC grid," Paris, Tech. Rep. CIGRE technical brochure 699, Sept. 2017.

[6] CIGRE WG B4.76, "DC-DC converters in HVDC grids and for connections to HVDC systems," Paris, Tech. Rep. CIGRE technical brochure 827, Mar. 2021.

[7] S. P. Engel, M. Stieneker, N. Soltau *et al.*, "Comparison of the modular multilevel DC converter and the dual-active bridge converter for power conversion in HVDC and MVDC grids," *IEEE Transactions on Power Electronics*, vol. 30, no. 1, pp. 124-137, Jan. 2015.

[8] G. J. Kish, M. Ranjram, and P. W. Lehn, "A modular multilevel DC/DC converter with fault blocking capability for HVDC interconnects," *IEEE Transactions on Power Electronics*, vol. 30, no. 1, pp. 148-162, Jan. 2015.

[9] G. J. Kish, "On the emerging class of non-isolated modular multilevel DC-DC converters for DC and hybrid AC-DC systems," *IEEE Transactions on Smart Grid*, vol. 10, no. 2, pp. 1762-1771, Mar. 2019.

[10] D. Jovcic, P. Dworakowski, G. Kish *et al.*, "Case study of non-isolated MMC DC-DC converter in HVDC grids," in *Proceedings of CIGRE Symposium*, Aalborg, Denmark, Jun. 2019, pp. 1-6.

[11] D. Jovcic and A. Jamshidifar, "Phasor model of modular multilevel converter with circulating current suppression control," *IEEE Transactions on Power Delivery*, vol. 30, no. 4, pp. 1889-1897, Aug. 2015.

[12] X. Lu, W. Lin, J. Wen *et al.*, "Dynamic phasor modelling and operating characteristic analysis of half-bridge MMC," in *Proceedings of IEEE 8th International Power Electronics and Motion Control Conference (IPEMC-ECCE Asia)*, Heifei, China, Jul. 2016, pp. 1-8.

[13] H. Yang, J. Qin, S. Debnath *et al.*, "Phasor domain steady-state modeling and design of the DC-DC modular multilevel converter," *IEEE Transactions on Power Delivery*, vol. 31, no. 5, pp. 2054-2063, Oct. 2016.

[14] H. Yang, M. Saeedifard, and A. Yazdani, "An enhanced closed-loop control strategy with capacitor voltage elevation for the DC-DC modular multilevel converter," *IEEE Transactions on Industrial Electronics*, vol. 66, no. 3, pp. 2366-2375, Mar. 2019.

[15] G. J. Kish and P. W. Lehn, "Linearized DC-MMC models for control design accounting for multifrequency power transfer mechanisms," *IEEE Transactions on Power Delivery*, vol. 33, no. 1, pp. 271-281, Feb. 2018.

[16] W. Lin and D. Jovcic, "Average modelling of medium frequency DC-DC converters in dynamic studies," *IEEE Transactions on Power Delivery*, vol. 30, no. 1, pp. 281-289, Feb. 2015.

[17] B. Dobrucky, M. Pokorny, and M. Benova, "Instantaneous single-phase system power demonstration using virtual two phase theory," in *Proceeding of 2008 IEEE International School on Nonsinusoidal Currents and Compensation*, Lagow, Poland, Jun. 2008, pp. 1-5.

[18] M. Janaszek, "Extended Clarke transformation for *n*-phase systems," *Proceedings of Electrotechnical Institute*, vol. 63, pp. 5-26, Dec. 2016.

[19] H. Zhang, D. Jovcic, W. Lin *et al.*, "Average value MMC model with accurate blocked state and cell charging/discharging dynamics," in *Proceeding of IEEE 4th International Symposium on Environmental Friendly Energies and Applications*, Belgrade, Serbia, Sept. 2016, pp. 1-6.

Aliakbar Jamshidi Far received the B.Sc., M.Sc., and Ph.D. degrees all in electrical engineering from Sharif University of Technology, Tehran, Iran, in 1992, Iran University of Science and Technology, Tehran, Iran, in 1996, and Amirkabir University of Technology, Tehran, Iran, in 2008. From 2008 to 2012, he was an Assistant Professor with Iranian Research Organization for Science and Technology. He joined University of Aberdeen, Aberdeen, UK, in 2012 as a Research Fellow, and is currently a Lecturer in electrical engineering. His research interests include high voltage direct current, renewable energy, and control systems.

Dragan Jovcic obtained a Diploma Engineer degree in control engineering from the University of Belgrade, Belgrade, Serbia, in 1993, and a Ph.D. degree in electrical engineering from the University of Auckland, Auckland, New Zealand, in 1999. He is currently a Professor with the University of Aberdeen, Aberdeen, UK, where he has been since 2004. In 2008, he held Visiting Professor post at McGill University, Montreal, Canada. He also worked as a Lecturer with University of Ulster, Ulster, UK, in the period 2000-2004 and as a Design Engineer in the New Zealand power industry, Wellington, New Zealand, in the period 1999-2000. His research interests include high voltage direct current, flexible AC transmission systems, and DC grids.